Front. Chem. China 2010, 5(1): 11–28
DOI 10.1007/s11458-009-0205-6

FEATURE ARTICLE

Theoretical studies on electronic spectroscopy and dynamics with the real-time time-dependent density functional theory

Jie LIU, Zhenyu GUO, Jin SUN and Wanzhen LIANG (✉)

Hefei National Laboratory for Physical Science at Microscale and Department of Chemical Physics, University of Science and Technology of China, Hefei 230026, China

Time-dependent density functional theory (TDDFT) has evolved into a general routine to extract the energies of low-lying excited states over the last decades. Driven by the remarkable progress of laser technology, the study of the interaction between matter and intense laser fields with ultrashort pulse duration develops rapidly. A great number of new strong field phenomena emerge. The requirement of a theoretical tool to study the intense field phenomena and dynamical processes of polyatomic systems is urgent. To extend the power of the TDDFT beyond the linear responses, an alternative scheme has been developed by numerically solving the time-dependent Kohn-Sham equations directly in real-time domain. In this article, we summarize the algorithms and capabilities of the real-time TDDFT on studying electron spectroscopy and dynamics of polyatomic systems. The failure of TDDFT with the adiabatic local-density approximation on some dynamical processes and the possible solutions are synopsized as well. The numerical implementation of algorithms and applications of RT-TDDFT on the linear and nonlinear spectroscopies and electronic dynamics of nano-size nonmetal clusters are displayed.

Keywords TDDFT, linear and nonliear optical spectroscopies, electron dynamics, intense field, HHG, interface charge transfer

1 Introduction

Time-dependent phenomena mainly originate from the interactions between the time-dependent external fields and materials, which can be classified into two types: (a) weak field interaction that is the interaction between the external field and molecules and is much weaker than the intra-molecular interaction, i.e., the radiation does not perturb the energy levels themselves and the system responds to the field linearly. (b) strong field interaction, in this case the intensity and frequency of the external field are comparative with the intra-molecular interaction and the natural time scale of electron. Hence the response of electron can not be treated with the perturbation theory.

Received August 27, 2009; accepted October 16, 2009
E-mail: liangwz@ustc.edu.cn

The dynamic properties that describe the response of systems to the external fields can be theoretically described by the time-dependent many-body wave functions, which are the solution of the systematic Schrödinger equation. However, the general solutions to the Schrödinger equation (TDSE) are not available, except for very simple cases like hydrogen molecule or like-hydrogen molecules. The time-dependent one-electron approaches, such as the time-dependent density functional theory (TDDFT) [1,2] and the random phases approximation time-dependent Hartree-Fock (TDHF) theory [3]. TDHF replaces the complicated many-body time-dependent Schrödinger equation by a set of time-dependent single-particle equations and therefore has evolved into a powerful tool for extracting electronic excited-state energies over the last decades due to the computational efficiency for the large-size systems. TDDFT comes from the generalization

of the original static Kohn-Sham density functional theory and TDHF from the mean-field Hartree-Fock theory, respectively. When they are implemented at the linear response level, a set of time-independent eigenvalue equations are derived [4–6]. This linear system possesses solutions for certain discrete eigenvalues. As a result, one obtains the energies by solving the eigenvalue equation. Currently, the routine has become the most general method to extract the energies of low-lying excited states [7–16] and to conduct geometrical optimization of excited states [17,18]. For simplicity, we denote this theory as the linear response (LR) theory.

TDDFT-LR, however, has its own limitations in the practical applications. For instance, it is computationally expensive and even impractical to deal with very complex systems. The reason is that one has to solve non-ordinary eigenvalue equation with a super matrix with the dimension of $(2N_{\mathrm{occ}}N_{\mathrm{nocc}}) \times (2N_{\mathrm{occ}}N_{\mathrm{nocc}})$, where N_{occ} and N_{nocc} are the number of occupied and unoccupied molecular orbitals. TDDFT-LR can not correctly deal with metal clusters since the orbitals nearby HOMO and LUMO are not disconnected clearly in these systems, hence it is hard to distinguish the different states explicitly. TDDFT-LR is also not suitable for studying atoms and molecules in intense laser pulse, where self-consistent non-perturbation, non-adiabatic approaches and real-time propagations are required.

Driven by the remarkable progress of laser technology [19], the study of the interaction between matter and intense laser fields with ultra-short pulse duration develops rapidly. The intense field phenomena, such as above-threshold ionization (ATI) [20], ultrahigh harmonic generation [21], and Coulomb explosion of molecules [22], have attracted a great number of experimental and theoretical researches. Currently a new field called attosecond science has formed. It probes the dynamical behavior of matter on the attosecond time scale (see Refs. [23–28]). The natural time scale of electrons falls into the subfemtosecond or attosecond regime, which is much shorter than the vibrational periods of atoms in molecules. Therefore, the progress of laser technology capable of reaching subfemtosecond or attosecond pulse durations has enabled us to capture and steer the electron motion inside atoms and molecules that are undergoing photoionization or chemical change. The quest to probe the intense-field phenomena and atomic and molecular electron dynamics on ultrashort timescales challenges the current theoretical approaches and stimulates people to develop a strategy to cope with non-adiabatic electron wave-packet dynamics. TDDFT theory, which can in principle produce the exact time-dependent electron density of many-body system, has therefore been developed to extend its capability to the intense field regime. In this case, an alternative scheme has been developed by numerically solving the time-dependent Kohn-Sham equations directly in real-time domain (RT-TDDFT) [12].

The quest to probe atomic and molecular electron dynamics on ultrashort timescales inevitably leads to the use of extreme ultraviolet (XUV)/X-ray radiation. High harmonic generation (HHG) and stimulated Raman scattering generate frequency components over a wide range [29–32] and thus are two techniques to produce attosecond light pulses. The HHG process, in which visible or infrared laser light is converted to vacuum ultraviolet radiation, was known for nearly two decades [21]. High harmonics from atoms have been extensively studied. An elegant and simple three-step quasi-static model has successfully interpreted atomic HHG [33]. The model could be described as follows: (1) tunnel ionization by an intense low-frequency laser field, (2) acceleration of the free electron, and (3) re-collision. However, it is still a challenge to explain the high harmonics generated from polyatomic molecules because the electron dynamics of molecules is more complicated than that in isolated atoms due to the multiple nuclei and their relative motions [34]. Besides, molecular harmonics are very sensitive to the molecular orientation, the spatial arrangement of atoms in the molecule and dynamic motion of the electrons [35,36]. The experiments on HHG of polyatomic molecules are thus far sparse. Several theoretical works have investigated the mechanism of HHG from polyatomic molecules using a variety of theoretical approaches. For example, Zhang [37] calculated HHG of C_{60} molecule using the time-dependent Hartree-Fock (TDHF) theory with a semi-empiricial Hamiltonian and concluded that HHG are mainly from the multiple excitations and are intrinsic to the system. Averbukh et al. [38] showed that molecular HHG by laser field is a result of "bound-bound" transitions rather than "bound-continuum" transitions, which dominate in the Corkum-Kulander recollision mechanism for atoms in a field. A more careful investigation on benzene has been performed by Baer et al. [39] applying time-dependent density functional theory (TDDFT) with the adiabatic local-density approximation. They found that for very strong fields (maximal strength larger than $3.5 \times 10^{14}\,\mathrm{W\cdot cm^{-2}}$), ionization ceases well before the pulse reaches maximum and the recollision event is not observed, while for the pulse with the moderate laser intensity (maximal strength smaller than $1\times10^{14}\,\mathrm{W\cdot cm^{-2}}$) the ionization continues throughout and the recollision event is observed. Therefore, the conjecture of Averbukh et al. [38] is that the dominant contribution to molecular HHG comes from the bound-bound transitions by using their model, which can only apply for stronger fields (above $1\times10^{14}\,\mathrm{W\cdot cm^{-2}}$).

TDSE governs the evolution of an entire isolated system, but unsolved questions arise when the entire system is divided into a quantum subsystem and its environment where the

quantum subsystem is described by a Schrödinger equation and its environment is described by classical mechanics. One notable example of a quantum-classical division is to treat electrons quantum mechanically and nuclei classically in studying the dynamical processes including laser-induced chemistry, dynamics at metal or semiconductor surfaces, and electron transfer. In these dynamical processes, the quantal electrons do not evolve adiabatically, hence leading to non-Born-Oppenheimer trajectories for nuclear motion. Two wildly used methods including nuclear effect based on TDSE are Ehrenfest dynamics [40–46] and surface hopping dynamics [47–49]. Ehrenfest dynamics replaces TDSE by (a) classical Newton's equations for nuclei (see Eq. (4)) and (b) TDSE for electrons. The surface-hopping approach includes nonadiabatic effect by allowing stochastic electronic transitions subject to a time- and momenta-dependent hopping probability. For a lager system, the surface-hopping method is computational demanding. RT-TDDFT allows one to observe the electron propagations in time and has coupled with the methods for nuclear motion to describe nonadiabatic electron wavepacket dynamics [40–44,50].

The goal of this review is to demonstrate the power of the RT-TDDFT on the time-dependent problems. Especially, we focus on our group's work on the development and application of RT-TDDFT to study the electron spectra and dynamics of nanosize clusters, such as finite-size C/BN nanotubes, bare carbon chain systems, and silicon clusters. Yabana and Bertsch developed a real-time real-space TDDFT scheme to calculate the optical responses of clusters [12]. Their pioneer work make it feasible to study molecular conductance, linear or nonlinear optical spectra, laser-driven intense field dynamics and ultrafast electron-nuclear dynamics, etc. [51–62] by the RT-TDDFT. TDDFT or TDHF theory, in its full extent without linear restrictions, can be applied directly to monitor the laser-driven electronic motion of multiphoton excitation with arbitrary laser pulse shape and duration. Therefore, they have been extensively used to study the intense field processes recently [37,39–44,63–77], although TDDFT with the adiabatic local-density approximation (ALDA) may not be fully suitable for the strong field process [78–80].

The paper is organized as follows. Section 2 summarizes the algorithms to solve the time-dependent one-electron equations with the density matrix and atom-centered basis functions. In Section 3, the linear and nonlinear spectra and electronic dynamics of finite-size C/BN nanotubes, bare carbon chain systems C_n, and nanosize silicon cluster are calculated and reported. The failure and the possible solutions of TDDFT with ALDA are presented. Finally, conclusions are given in Section 4.

2 RT-TDDFT scheme

The time-dependent full Schrödinger equation for a general electron-ion system can be written as:

$$\mathrm{i}\hbar\frac{\partial\Phi(\{\mathbf{r}_i\},\{\mathbf{R}_I\},t)}{\partial t}=H(\{\mathbf{r}_i\},\{\mathbf{R}_I\},t)\Phi(\{\mathbf{r}_i\},\{\mathbf{R}_I\},t); \quad (1)$$

where $\mathbf{r}$ and $\mathbf{R}$ are the positions of the electrons and the nuclei, respectively. $\Phi(\{\mathbf{r}_i\},\{\mathbf{R}_I\},t)$ is the total wave function and H is the time-dependent Hamiltonian of electron-ion system written as:

$$\begin{aligned}&H(\{\mathbf{r}_i\},\{\mathbf{R}_I\},t)\\&=-\sum_I\frac{\hbar^2}{2M_I}\nabla_I^2-\sum_i\frac{\hbar^2}{2m}\nabla_i^2+\frac{1}{2}\sum_{I\neq J}\frac{Z_IZ_J}{|\mathbf{r}_i-\mathbf{R}_I|}\\&+\frac{1}{2}\sum_{j\neq i}\frac{e^2}{|\mathbf{r}_i-\mathbf{r}_j|}+V_{\mathrm{ext}}(\{\mathbf{r}_i\},\{\mathbf{R}_I\},t).\end{aligned} \quad (2)$$

Here m and e denote the mass and the charge of the electron, M_I and Z_I are the mass and nuclear charge of the I-th nuclear, respectively. V_{ext} denotes the interaction between the matter and the external field. In order to build up the equation of motion for both the electrons and the nuclei at the density functional theory (DFT) level, the Lagrangian is constructed as:

$$\begin{aligned}\mathscr{L}=&\sum_I\left(\frac{1}{2}M_I\dot{\mathbf{R}}_I^2+Z_I\mathbf{R}_I\mathcal{E}(t)\right)-\frac{1}{2}\sum_{I\neq J}\frac{Z_IZ_J}{|\mathbf{R}_I-\mathbf{R}_J|}\\&+\sum_i\left\langle\phi_i\left|\mathrm{i}\hbar\frac{\partial}{\partial t}-e\mathbf{r}_i\cdot\mathcal{E}(t)\right|\phi_i\right\rangle-E_{\mathrm{elec}}^{\mathrm{DFT}}(\{\mathbf{r}_i\},\{\mathbf{R}_I\},t)\end{aligned} \quad (3)$$

Here ϕ_i is Kohm-Sham orbitals, $E_{\mathrm{elec}}^{\mathrm{DFT}}$ is usual DFT energy functional and $\mathcal{E}(t)$ is the amplitude of the time-dependent external filed. Variation of Lagrangian for the nuclear coordinates $\mathbf{R}_I$ and the orbital variables $\phi_i(t)$, the classical Newton's equation of motion for $\mathbf{R}_I$, and the usual TDKS equation are separately given as:

$$\begin{aligned}M_I\frac{\mathrm{d}^2\mathbf{R}_I}{\mathrm{d}t^2}=&Z_I\mathcal{E}(t)-\frac{1}{2}\sum_{I\neq J}\frac{Z_IZ_J(\mathbf{R}_I-\mathbf{R}_J)}{|\mathbf{R}_I-\mathbf{R}_J|^3}\\&-\Delta_IE_{\mathrm{elec}}^{\mathrm{DFT}}(\{\mathbf{r}_i\},\{\mathbf{R}_I\},t),\end{aligned} \quad (4)$$

and

$$\mathrm{i}\frac{\partial\phi_i(r,t)}{\mathrm{d}t}=\left(-\frac{1}{2}\nabla^2+v_{\mathrm{s}}[n(\mathbf{r},t)](\mathbf{r},t)\right)\phi_i(\mathbf{r},t). \quad (5)$$

The single electron effective potential is defined as:

$$v_{\mathrm{s}}(\mathbf{r},t)=v_{\mathrm{ext}}(\mathbf{r},t)+v_{\mathrm{hartree}}(\mathbf{r},t)+v_{\mathrm{xc}}(\mathbf{r},t). \quad (6)$$

Here $v_{\mathrm{xc}}(\mathbf{r},t)$ is the exchange and correlation potential,

producing the same time-dependent density as the exact one. v_{ext} is the external potential. When the term $v_{xc}(\mathbf{r},t)$ only includes the exact HF exchange term, TDKS equation becomes TDHF equation.

2.1 Propagation of the reduced one-electron density matrix

Casting TDKS equation into the reduced one-electron density matrix (1DM) form, one gets an alternative form of the TDDFT equation in terms of the generalized nonorthogonal atomic orbital (AO) basis sets as [81]:

$$\mathrm{i}S\frac{\mathrm{d}\rho'(t)}{\mathrm{d}t}S = F'(t)\rho'(t)S - S\rho'(t)F'(t) \tag{7}$$

with the Fock operator $F[n(\mathbf{r}, t)]$ given by

$$F'[n(\mathbf{r},t)](\mathbf{r},t) = -\frac{1}{2}\nabla^2 + v_s[n(\mathbf{r},t)](\mathbf{r},t). \tag{8}$$

With respect to some orthogonalization procedures, such as the Löwdin or Cholesky decomposition orthogonalization procedure, one can transform the AO Fock matrix F' and the AO density matrix ρ' into an orthonormal basis form. For example in Cholesky decomposition, the overlap matrix S is decomposed into lower and upper triangle matrices as $S = LL^{\mathrm{T}}$. Then one gets $F = L^{-1}F'L^{-\mathrm{T}}$ and $\rho = L^{\mathrm{T}}\rho'L$ [82]. In an orthogonal form, Eq. (7) becomes the standard Liuviolle equation

$$\mathrm{i}\frac{\mathrm{d}\rho(t)}{\mathrm{d}t} = [F(t),\rho(t)] = \mathscr{L}(t)\rho(t). \tag{9}$$

Decompose the matrix form of the Liuviolle operator into $\mathscr{L}(n(\mathbf{r},t)) = \mathscr{L}_0(n_0) + \mathscr{L}'(n(\mathbf{r},t))$, where $\mathscr{L}' = \mathscr{L}_{ext} + \mathscr{L}(\delta n(\mathbf{r},t))$. If we let $\rho = \exp(-\mathrm{i}\mathscr{L}_0 t)\sigma$, we obtain

$$\mathrm{i}\frac{\mathrm{d}\sigma(t)}{\mathrm{d}t} = \mathrm{e}^{-\mathrm{i}t\mathscr{L}_0}\mathscr{L}'\,\mathrm{e}^{\mathrm{i}t\mathscr{L}_0}\sigma(t), \tag{10}$$

which we integrated as

$$\sigma(t) = \sigma_i - \mathrm{i}\int_{t_i}^{t}\mathrm{d}\tau\mathrm{e}^{-\mathrm{i}t\mathscr{L}_0}\mathscr{L}'\,\mathrm{e}^{\mathrm{i}t\mathscr{L}_0}\sigma(\tau) = \sigma_i + \delta\sigma(t), \tag{11}$$

where σ_i denotes σ at $t = t_i$.

To solve Eq. (9) or Eq. (10) in real-time domain, one encounters an explicitly time-dependent problem. A common strategy is to propagate the reduced density matrix step by step with a small enough time step-size. Within each time-step, the effective Hamiltonian is assumed to be stationary. A variety of short-time propagation approaches are currently available for this explicitly time-dependent problem (see reviews, e.g., Refs. [83,84]). However, the RT-TDDFT scheme requires one to build the effective Hamiltonian at least once at each time step. The effective Hamiltonian construction is the most computational time-consuming part. Therefore, in order to efficiently solve the TDDFT equation using the short time propagator, one should use both fast approaches to construct the Hamiltonian and good approximate methods to calculate the evolution operators, which allows the time step-size as large as possible.

Algorithms whose computational cost scales linearly only asymptotically with the size of the molecule are currently available for the effective Hamiltonian construction in DFT. The success of these methods means that effective Hamiltonian construction (which was previously the computationally dominant step) is now no longer necessarily at least for large molecules. For adequate large molecules, the calculation of evolution operators may become the rate-determining step. In our previous work [85], we therefore focused on assessing the propagation schemes. In particular, we investigated the low-order Magnus integration method [86] and the Krylov-subspace method [87]. The relative methods will be described below.

In Ref. [85], we have described some of the algorithms that can be used to solve Eq. (9) or Eq. (10) step by step. Here we introduce them in more details. The solution of Eq. (9) can be written as

$$\rho(t) = U(t,t_0)\rho(t_0)U(t_0,t), \tag{12}$$

where the initial state $\rho(t_0)$ can be obtained from a usual ground state calculation and U is the evolution operator, which satisfies

$$\mathrm{i}\hbar\frac{\partial}{\partial t}U(t,t_0) = FU(t,t_0), \tag{13}$$

with $U(t_0, t_0) = 1$. The formal solution of Eq. (13) can be written as

$$U(t,t_0) = \mathcal{T}\exp\left\{-\mathrm{i}\int_{t_0}^{t}\mathrm{d}\tau F(\tau)\right\}, \tag{14}$$

where $\mathcal{T}$exp is time order exponential. In principle, Eq. (9) can be straightforwardly solved by using tools for the ordinary differential equation. One of the well-known methods is the Runge-Kutta algorithm [88]. However, the low-order Runge-Kutta method requires a rather small time step-size to maintain the idempotency constraint on the density matrix. In the higher-order method, the Fock matrix would be constructed several times at each time step. Therefore, it is very expensive for the practical calculations. Alternative schemes are adopted to solve Eq. (9).

2.1.1 Magnus integration method

As Δt is small enough, $U(t_0 + \Delta t, t_0)$ can be written as [89]

$$U(t_0 + \Delta t,t_0) = \mathrm{e}^{\hat{Q}(\Delta t)} \quad \text{Magnus} \tag{15}$$

$$= \left[I - \frac{1}{2}C(\Delta t)\right]^{-1}\left[I + \frac{1}{2}C(\Delta t)\right] \quad \text{Cayley} \tag{16}$$

Here, "Magnus" denotes the classical Magnus analytical expansions [90], and "Cayley" represents the Cayley transform [91] with $\frac{1}{2}C(\Delta t) = \left(e^{\hat{Q}(\Delta t)} + I\right)^{-1}\left(e^{\hat{Q}(\Delta t)} - I\right)$. $\hat{Q}(t + \Delta t,t)$ can be expanded by an infinite series

$$\hat{Q}(t + \Delta t,t) = \sum_{k=1}^{\infty}\hat{Q}_k(t + \Delta t,t) \tag{17}$$

where $\hat{Q}_k$ is generated by

$$\hat{Q}_k(t + \Delta t,t) = \sum_{j=0}^{k-1}\frac{B_j}{j!}\int_t^{t+\Delta t}\hat{S}_k^j(\tau)\mathrm{d}\tau \tag{18}$$

Here B_j are Bernoulli numbers and $\hat{S}$ can be computed as

$$\hat{S}_1^0(\tau) = -\mathrm{i}\hat{H}(\tau);\ \hat{S}_k^0(\tau) = 0(k > 1); \tag{19}$$

$$\hat{S}_k^j(\tau) = \sum_{m=1}^{k-j}\left[\hat{Q}_m(t + \Delta t,t),\hat{S}_{k-m}^{j-1}(\tau)\right](1 \leqslant j \leqslant k-1). \tag{20}$$

The first two term of $\hat{Q}_k(t + \Delta t,t)$ are

$$\hat{Q}_1(t + \Delta t,t) = \int_t^{t+\Delta t}\mathrm{d}\tau_1\left[-\mathrm{i}\hat{F}(\tau_1)\right] \tag{21}$$

$$\hat{Q}_2(t + \Delta t,t) = \int_t^{t+\Delta t}\mathrm{d}\tau_1\int_t^{\tau_1}\mathrm{d}\tau_2\left[-\mathrm{i}\hat{F}(\tau_1),-\mathrm{i}\hat{F}(\tau_2)\right] \tag{22}$$

Truncating the Magnus series to n-th order, a method of order $2n$ is obtained. When n = 1, the second-order Magnus expansion is

$$\hat{Q}_{M(2)}(t + \Delta t,t) = -\mathrm{i}\hat{H}(t + \Delta t/2)\Delta t. \tag{23}$$

When n = 2, the fourth-order Magnus expression is able to be constructed,

$$\hat{Q}_{M(4)}(t + \Delta t,t) = -\mathrm{i}\frac{\Delta t}{2}\left[\hat{H}(t_1) + \hat{H}(t_2)\right] - \frac{\sqrt{3}\Delta t^2}{12}\left[\hat{H}(t_2),\hat{H}(t_1)\right], \tag{24}$$

where $t_{1,2} = t + [(1/2) \mp \sqrt{3}/6]\Delta t$ are the Gauss quadrature sampling points. One commutator exists in the fourth-order Magnus expansion. Moreover, the number of such commutators will grow rapidly with increasing order.

2.1.2 Time-reversal symmetry based propagator

It is obvious that the second-order Magnus expansion can be regarded as the exponential midpoint rule

$$\hat{U}_{\mathrm{EM}}(t + \Delta t,t) = \exp\left\{-\mathrm{i}\Delta t\hat{H}(t + \Delta t/2)\right\}. \tag{25}$$

In a time-evolving problem, $\phi(t + \Delta t/2)$ can either be obtained by propagating backwards $\Delta t/2$ starting from $\phi(t + \Delta t)$ or propagating forwards $\Delta t/2$ starting from ϕ(t). Then we can obtain time-reversal symmetry (TRS) method:

$$\exp\left\{\mathrm{i}\frac{\Delta t}{2}\hat{H}(t + \Delta t)\right\}\varphi(t + \Delta t) = \exp\left\{-\mathrm{i}\frac{\Delta t}{2}\hat{H}(t)\right\}\varphi(t). \tag{26}$$

Multiplying both side by $\exp\left\{-\mathrm{i}\frac{\Delta t}{2}\hat{H}(t + \Delta t)\right\}$, one gets

$$\hat{U}_{\mathrm{ETRS}}(t + \Delta t,t) = \exp\left\{-\mathrm{i}\frac{\Delta t}{2}\hat{H}(t + \Delta t)\right\} \times \exp\left\{-\mathrm{i}\frac{\Delta t}{2}\hat{H}(t)\right\}. \tag{27}$$

It is obvious that this method is time reversible.

2.1.3 Splitting techniques (ST)

Watanabe and Tsukada [92] have combined the EM approximation with the split-operator method. In principle, it is able to obtain a second-order method but requires $\hat{V}(t + \Delta t/2)$ computed accurately. A simple alternative method to obtain an order 2 method,

$$\hat{U}_{\mathrm{SO}}(t + \Delta t,t) = S_2\left[-\mathrm{i}\Delta t\left(\hat{T} + \hat{V}'\right)\right] = \exp\left\{-\frac{1}{2}\mathrm{i}\Delta t\hat{T}\right\} \times \exp\left\{-\mathrm{i}\Delta t\left[\hat{V}'_{\mathrm{int}}[\rho'] + \hat{V}_{\mathrm{ext}}(t + \Delta t/2)\right]\right\} \times \exp\left\{-\frac{1}{2}\mathrm{i}\Delta t\hat{T}\right\}, \tag{28}$$

where ρ' is not the density $\rho(t + \Delta t/2)$, but the density applies the first kinetic term,

$$\rho' = \sum_{n=1}^{N}\left|\exp\left\{-\frac{1}{2}\mathrm{i}\Delta t\hat{T}\right\}\varphi_n(t)\right|^2. \tag{29}$$

Associating ρ' with $\rho(t + \Delta t)$, it is easy to prove this method is of order 2.

For the fourth-order ST technique, a time-dependent version is suggested by Suzuki et al. [69,70],

$$\hat{U}_{\mathrm{ST}}(t + \Delta t,t) = \prod_{j=1}^{5}S_2\left[-\mathrm{i}p_j\Delta t\hat{H}(t_j)\right], \tag{30}$$

where the times t_j are related to the set p_j through $t_j = t + (p_1 + \ldots + p_j/2)\Delta t$. And $p_5 = p_1$, $p_4 = p_2$, $p_1 = p_2 = \frac{1}{4 - 4^{1/3}}$, $p_3 =$

$1-4p_1$. If the potential between t and $t+\Delta t$ has been computed accurately, this method is of order 4 technique.

2.1.4 Krylov-subspace scheme

The evolution of the density matrix can be expressed as $\rho(t) = \mathrm{e}^{-\frac{\mathrm{i}}{\hbar}\mathscr{L}\Delta t}\rho(t_0)$ in the time internal $[t_0, t_0 + \Delta t]$. A projection of the matrix exponential $\mathrm{e}^{-\frac{\mathrm{i}}{\hbar}\mathscr{L}\Delta t}$ in Krylov subspaces can be applied. The conventional Krylovsubspace scheme may be generalized to adopt the non-Hermitian Hamiltonian. In this work we adopt the short iterative-Arnoldi method which has been developed by Pollard and Friesner [87]. The essence of that propagation method is to form an explicit representation of the exponential operator $\mathrm{e}^{\frac{-\mathrm{i}}{\hbar}\mathscr{L}\Delta t} = \mathrm{e}^{L\Delta t}$ in the n-dimensional Krylov space based on the initial density matrix $\rho(t_0)$. The method is defined by the recurrence relation

$$h_{j+1,j}v_{j+1} = Lv_j - \sum_{i=0}^{j} h_{i,j}v_i, \tag{31}$$

where v_i is the i-th orthonormal basis vector and $h_{i,j}$ is a matrix element of L in this basis. This transformation of L may be written, $L \approx VhV^{\mathrm{T}}$, where V is the orthogonal matrix whose j-th column is v_j. The $\{v_j\}$ are constructed iteratively. Setting $v_0 = \rho(t_0)$ and diagonalizing h, we can express $\rho(t) = \mathrm{e}^{Lt}\rho(t_0) \approx VW\mathrm{e}^{\Lambda t}W^{-1}V^{\mathrm{T}}v_0$ where $hW = W\Lambda$.

2.1.5 Approximation to the exponential of a matrix

It is noted that Castro et al. [54] have extensively investigated the propagation schemes to solve the time-dependent Kohn-Sham orbitals in the grid representation. In our work, however, we propagate the reduced density matrix in AO basis representation. The time evolution of the one-electron density matrix is calculated. The finite-size atom-centered Gaussian orbitals are used. The reduced 1DM in AO basis possesses the localized properties for large molecules. For this case, one explicit problem we encountered is to calculate the matrix exponential e^{Q}.

To calculate the matrix exponential e^{Q}, the exact method is to straightforwardly diagonalize the matrix Q. It, however, is only applicable to small systems. For complex systems, one has to develop approximate approaches. One typical approach is to apply the MP or CMP expansion of matrix exponentials.

$$\mathrm{e}^{Q} = U\mathrm{e}^{q}U^{\dagger}, \quad QU = qU \quad \text{Matrix diagonalization} \tag{32}$$

$$\mathrm{e}^{Q} = \sum_{n=0}^{k_{\max}} \frac{1}{n!}Q^n \quad \text{MP}, \tag{33}$$

$$= \sum_{n=0}^{k_{\max}} (2-\delta_{n0})(-\mathrm{i})^n J_n(\Delta t)T_n(F_{\mathrm{norm}}), \quad \text{CMP} \tag{34}$$

Here, T_n is the CMP and can be generated using the recursion formula [84]. J_n is the Bessel function. F_{norm} is the scaled and shifted F matrix, defined so that its eigenvalues lie in the interval $[-1, 1]$ to satisfy the definition of the Chebyshev polynomials. Explicitly, F_{norm} is given by $\dfrac{F-\overline{E}}{\Delta E/2}$ with $\Delta E = E_{\max} - E_{\min}$, and $\overline{E} = (E_{\max} + E_{\min})/2$, where $E_{\min}$ and $E_{\max}$ are the minimum and maximum eigenvalues of the Fock matrix F.

As Δt is sufficiently small, the second order Magnus expansion can predict the convergent results. However, even if the second order algorithm is used, one still needs to know $F(t_0+\Delta t/2)$ which depends on the unknown reduced one-electron density matrix $\rho(t_0 + \Delta t/2)$. Ref. [56] suggests a predictor-corrector scheme to evaluate $F(t_0+ \mathrm{d}t/2)$ without using $\rho(t_0 +\Delta t/2)$. It has been successful in describing the conductance within the TDDFT. We will adopt this method in the later numerical test and applications. Once $F(t_0+ \mathrm{d}t/2)$ is known, $\mathrm{e}^{F/\mathrm{i}\hbar}$ can be calculated with respect to the MP/CMP expansion. In order to speed up the calculation of e^{Q}, we use the fast method for summing MP and CMP [82,93], which can significantly reduce the number of matrix multiplies from $k_{\max} - 1$ to about $2\sqrt{k_{\max}}$.

2.2 Propagation of nuclei

To perform the propagation of nuclei, one has to evaluate the forces, i.e., the gradient of electron energy. The electron energy formula based on 1DM $\rho' = \rho'^{\alpha} + \rho'^{\beta}$ is written as

$$E = \mathrm{Tr}(\rho' h') + \frac{1}{2}\mathrm{Tr}(\rho' G'(\rho')) + E_{\mathrm{xc}}. \tag{35}$$

Here h' is the one-electron part of Hamiltonian. $G'(\rho') = J'(\rho') + C_{\mathrm{HF}}K'(\rho')$ with the elements of G' matrix follows:

$$J'(\rho')_{\mu\nu} = \sum_{\gamma,s} \rho'_{\gamma,s}V_{\mu\gamma;\nu s} \tag{36}$$

$$K'(\rho')_{\mu\nu} = \sum_{\gamma,s} \rho'_{\gamma,s}V_{\mu\gamma;s\nu}. \tag{37}$$

V is the four-center two-electron Coulomb integrals with elements

$$V_{\mu\gamma;\nu s} = \int \mathrm{d}\mathbf{r}_1 \int \mathrm{d}\mathbf{r}_2 \chi^*_{\mu}(\mathbf{r}_1)\chi^*_{\gamma}(\mathbf{r}_2)\frac{e^2}{|\mathbf{r}_1-\mathbf{r}_2|}\chi_{\nu}(\mathbf{r}_1)\chi_{s}(\mathbf{r}_2). \tag{38}$$

χ_μ are the atomic orbital (AO) wave functions, and $\mathbf{r}$ is the displacement vector of an electron. E_{xc} is the pure DFT

exchange-correlation energy. In HF approximation, $E_{xc} = 0$ and $C_{HF} = -1/2$.

Differentiating the SCF energy expression with respect to nuclear displacement R leads to the following expression

$$\frac{\partial E}{\partial R} = \mathrm{Tr}(\rho' h'^{\mathrm{R}}) + \frac{1}{2}\mathrm{Tr}(\rho' G'^{(\mathrm{R})}(\rho')) + \mathrm{Tr}(\rho'^{\mathrm{R}} F') + E_{xc}^{(\mathrm{R})}. \quad (39)$$

Enclosing a parameter in parentheses means that only the explicit dependence on the parameter is differentiated.

Unlike in SCF procedure, in order to evaluate Eq. (39), one has to know the derivative of ρ'. The procedure [94] of Voth et al. may be used to evaluate the term of $\mathrm{Tr}(\rho'^{\mathrm{R}} F')$. Then Eq. (39) reads as

$$\frac{\partial E}{\partial R} = \mathrm{Tr}(\rho' h'^{\mathrm{R}}) + \frac{1}{2}\mathrm{Tr}(\rho' G'^{(\mathrm{R})}(\rho')) + E_{xc}^{(R)} - \mathrm{Tr}\left[F\frac{\mathrm{d}L^{\mathrm{T}}}{\mathrm{d}R}L^{-\mathrm{T}}\overline{\rho} + \overline{\rho}L^{-1}\frac{\mathrm{d}L}{\mathrm{d}R}F\right] \quad (40)$$

with $\overline{\rho} = 2\rho^2 - 3\rho^3$. And for the Lowdin orthogonalization,

$$\frac{\mathrm{d}\mathscr{L}}{\mathrm{d}R} = \sum_{i,j} L_i \frac{1}{l_i^{1/2} + l_j^{1/2}}\left(L_i^{\mathrm{T}}\frac{\mathrm{d}S}{\mathrm{d}R}L_j\right)L_j^{\mathrm{T}}, \quad (41)$$

where l_i and L_i are the i-th eigenvalue and eigenvector of the overlap matrix S. For the Cholesky orthogonalization,

$$\left[\frac{\mathrm{d}L}{\mathrm{d}R}L^{-1}\right]_{i,j} = \begin{cases} \left(L^{-\mathrm{T}}\frac{\mathrm{d}S}{\mathrm{d}R}L^{-1}\right)_{i,j}, & i < j \\ \frac{1}{2}\left(L^{-\mathrm{T}}\frac{\mathrm{d}S}{\mathrm{d}R}L^{-1}\right)_{i,j}, & i = j \\ 0, & i > j. \end{cases} \quad (42)$$

3 Applications of RT-TDDFT

3.1 Linear or nonlinear optical spectra

When the external field interacts with matter, absorption and emission spectra are determined by the time-dependent dipole moment and hence are the important tools to describe the behavior of electronic dynamics. In this section, we demonstrate how to calculate the linear or nonlinear optical spectra by means of RT-TDDFT.

3.1.1 Dynamic polarizability

The electron polarization P is expressed as

$$P(t) = \langle\Phi(t)|\hat{P}|\Phi(t)\rangle, \quad (43)$$

where $\Phi(t)$ is the systematic many-body wavefunction. P may be expanded in powers of external field as

$$P(t) = P^{(0)} + P^{(1)} + P^{(2)} + P^{(3)} + \cdots = P^{(0)} + \chi^{(1)} : E + \chi^{(2)} : E^2 + \chi^{(3)} : E^3 + \cdots \quad (44)$$

with the n-th order polarization (n = 1, 2, 3, …)

$$P^{(n)} = \mathrm{Tr}\left(\hat{P}\delta\rho^{(n)}\right). \quad (45)$$

Here the trace Tr is over all the atomic orbitals. $P^{(1)}$, $P^{(2)}$, and $P^{(3)}$ are the linear, second- and third-order polarizations, respectively. $\chi^{(1)}$, $\chi^{(2)}$, and $\chi^{(3)}$ are the first-, second-, and third-order polarizabilities, respectively.

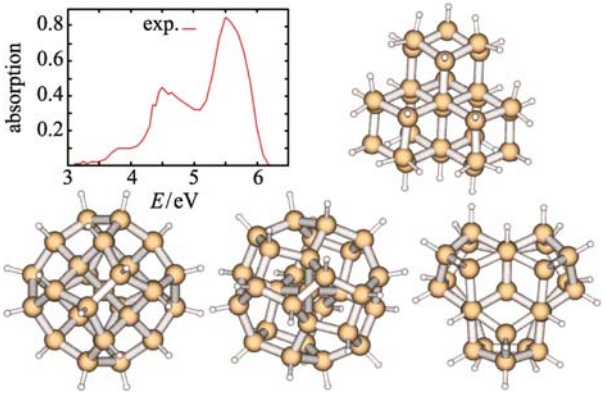

Figure 1 The experimental absorption spectrum and geometries of silicon clusters $Si_{29}H_x$. The structures at bottom are the ideal bulk-like configuration $Si_{29}H_{24}$, two nano-particles $Si_{29}H_{24}^{nano1}$ and $Si_{29}H_{24}^{nano2}$ (from left to right). The geometry of $Si_{29}H_{36}$ is shown in the upper right.

The field-induced 1DM $\delta\rho(t) = \delta\rho^{(1)}(t) + \delta\rho^{(2)}(t) + \delta\rho^{(3)}(t) + \cdots$ can be solved order-by-order in time-domain as follows [95]:

$$\mathrm{i}\frac{\mathrm{d}\delta\rho^{(1)}(t)}{\mathrm{d}t} = [F^{(0)},\delta\rho^{(1)}(t)] + [\delta F^{(1)}(t),\delta\rho^{(0)}],$$

$$\mathrm{i}\frac{\mathrm{d}\delta\rho^{(2)}(t)}{\mathrm{d}t} = [F^{(0)},\delta\rho^{(2)}(t)] + [\delta F^{(1)}(t),\delta\rho^{(1)}(t)] + [\delta F^{(2)}(t),\delta\rho^{(0)}],$$

$$\mathrm{i}\frac{\mathrm{d}\delta\rho^{(3)}(t)}{\mathrm{d}t} = [F^{(0)},\delta\rho^{(3)}(t)] + [\delta F^{(1)}(t),\delta\rho^{(2)}(t)] + [\delta F^{(2)}(t),\delta\rho^{(1)}(t)] + [\delta F^{(3)}(t),\rho^{(0)}].$$

$\delta F^{(n)}(t)$ is the n-th order induced Fock matrix and the first order matter-field interaction term is involved by $\delta F^{(1)}(t)$:

$$\delta F^{(1)}(t) = F(\delta\rho^{(1)}(t)) - \boldsymbol{\mu}\cdot\boldsymbol{E}(t). \quad (46)$$

Once we know n-th induced density matrix $\delta\rho^{(n)}$, $P^{(n)}(t)$ can be evaluated, the n-th dynamic polarizability is obtained [95].

In the following we demonstrate how to calculate the absorption cross section by RT-TDDFT. It is known that the absorption cross section is proportional to $\chi^{(1)}$ as

$$\sigma(\omega) \propto \omega \mathrm{Im}(\chi_{ij}^{(1)}(\omega)). \tag{47}$$

Here the dynamic polarizability tensor $\chi_{ij}^{(1)}(\omega) = \dfrac{\partial P_i^{(1)}(\omega)}{\partial \varepsilon_j(\omega)}$, and $P_i(\omega)$ denotes the Fourier transform of $P_i(t) = \mathrm{Tr}(\rho(t)\mu_i)$, where μ_i stands for the i-th component of the dipole moment.

As an application, we have calculated the absorption spectra of silicon nano-particles $Si_{29}H_x$ [85]. The optical properties of Si nano-particles with the size of 1 nm were experimentally measured [96]. The experiment showed that the particles exhibit three distinct excitation bands centered at 275, 310, and 335 nm (corresponding to 4.6, 4.0 and 3.7 eV, respectively). Four conformations of Si nano-particles with the size of 1 nm can be constructed, including the bulk construction of $Si_{29}H_{36}$, the ideal bulklike and two non-bulklike reconstruction configurations of the filled fullerene single-core $Si_{29}H_{24}$ (see Figure 1). It is interesting for us to know which construction contributes to the observed absorption bands.

In the calculation of absorption spectrum, the weak Gaussian envelope external electric field, $\varepsilon(t) = \dfrac{E_0}{\sqrt{\pi}\tau} \mathrm{e}^{-(t-\bar{t})^2/\tau^2}$, with the amplitude $E_0 = 1.0\times10^{-4}$ a.u., $\bar{t} = 0.0$ and $\tau = 4.0$ a.u. is applied. The second-order Magnus algorithm is used to approximate the evolution operator, and the MP expansion is used to approximate the matrix exponential. The density matrix is propagated without the nuclear motion. Effective core potential lanl2dz [97] is used for atom silicon, and 6-31G** basis set is used for atom H. A locally modified version of Quantum Chemistry Package Q-chem [98] is used. The system is evolved from $T = -10$ a.u. to $T = 1500$ a.u. The damping factor $\gamma = 0.004$ a.u. is assumed.

The popular hybrid XC functional B3LYP and GGA XC functionals, BP and BLYP, were used to check the efficiency of DFT functionals in describing the optical properties of nano-particles. It is found that the calculated absorption spectrum of bulk-like configuration $Si_{29}H_{24}$ (see Figure 2) with respect to B3LYP XC functional agrees exactly with experimental measurement of 1 nm Si nano-particles [96]. The silicon particles with sizes of 1 nm and the optical excitations at 3.7, 4.0 and 4.6 eV may consist of 29 Si atoms surrounded by 24 hydrogen atoms not by 36 hydrogen atoms.

3.1.2 HHG spectra of polyatomic systems

HHG can be viewed as the power radiated by a system in the strong field. It can be approximately evaluated by means of the quasi-classical Larmor formula [99]

$$P(t) = \frac{2e^2}{3c^3}|\ddot{d}(t)|^2, \tag{48}$$

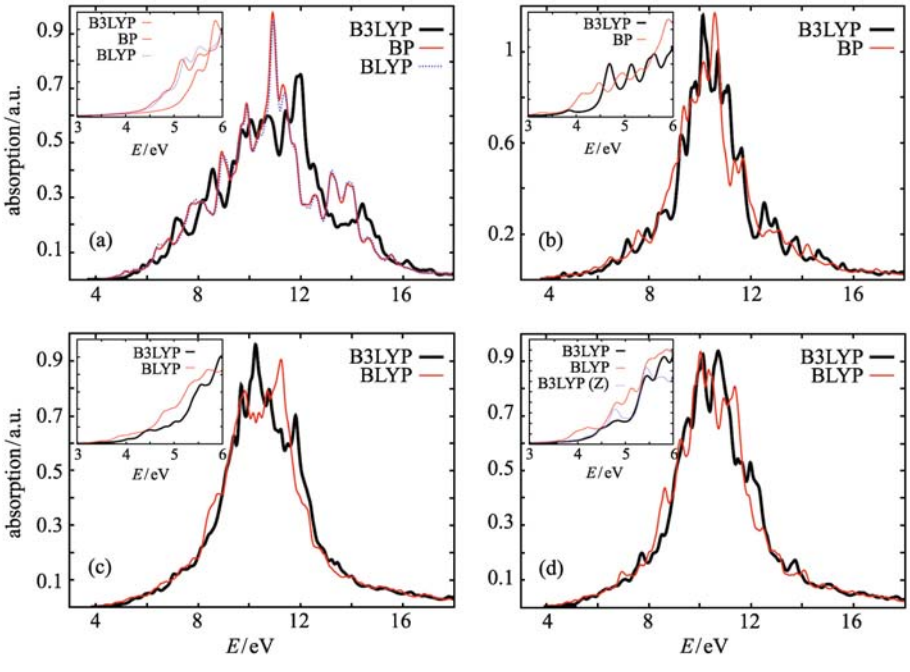

Figure 2 The absorption spectra of bulk cluster (a) $Si_{29}H_{36}$, (b) bulklike $Si_{29}H_{24}$, (c) $Si_{29}H_{24}^{nano1}$, and (d) $Si_{29}H_{24}^{nano2}$.

where c is the speed of light, and $\ddot{d}(t)$ is the electron acceleration defined as

$$\ddot{d}(t) = \frac{1}{m}\frac{\mathrm{d}^2\langle\Phi(\mathbf{r},t)|\hat{\mu}|\Phi(\mathbf{r},t)\rangle}{\mathrm{d}t^2}. \quad (49)$$

With the 1DM ρ, the dipole acceleration can be alternatively written as

$$\ddot{d}(t) = \frac{\mathrm{d}^2}{\mathrm{d}t^2}\mathrm{Tr}(\rho(t)\mu). \quad (50)$$

In this case, Eq. (9) should be solved in its full extent without linear restrictions. The finite difference method is used to calculate $\ddot{d}(t)$ in our work [100–102]. Based on the time-dependent one-electron approaches, we have studied the interaction of both the LP and CP laser pulses with finite-size Carbon nanotubes [100], Boron-nitride (BN) nanotubes [101], and the linear and cyclic structure carbon clusters C_n [102]. The polarized laser pulse is specified by $E(t) = E_{\max}\varepsilon(t)\cdot\left(\cos(\omega t)\hat{i} + \lambda\sin(\omega t)\hat{j}\right)$ with the pulse shape function $\varepsilon(t) = \sin^2(\pi t/t_\mathrm{p})$. Here t_p denotes the total duration of the laser pulse. $\lambda = 0$ is for the LP laser pulse and $\lambda = \pm 1$ for the left/right CP laser pulses. The polarization direction of LP laser field is set along the long chain and that of CP laser field is set to be perpendicular to the N-fold rotational symmetry axis of cyclic structures.

Figures 3, 4 and 5 show the calculated harmonics spectra generated by the linear chain C_9 and cyclic structure C_{10}, respectively. The hybrid exchange-correlation functional B3LYP [103] and the effective core potential (ECP) CRENBL [104] were applied. When C_9 and C_{10} are exposed to a LP laser field directed along the long chain, we only observe the odd-order harmonics without exception due to the inversion symmetry of molecules. A relatively weak laser pulse can generate efficient HHG for carbon chains. The maximal harmonic orders can be extended to 10-th in C_9 even if the laser intensity is as weak as 1.4×10^{13} W·cm^{-2} ($|E_{\max}| = 0.02$ a.u.).

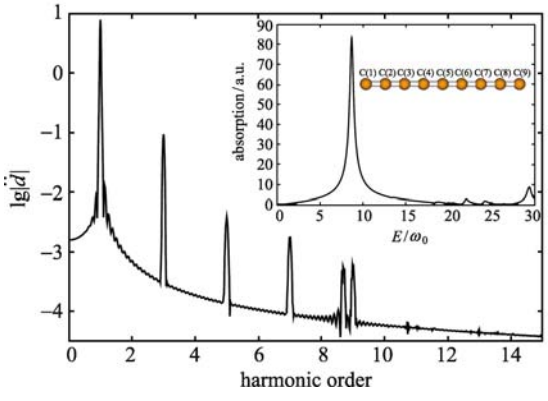

Figure 3 Harmonics generated by C_9 in LP field with $\omega_0 = 0.02$, $E_{\max} = 0.02$ and the pulse duration $t_\mathrm{p} = 50\tau\left(\tau = \frac{2\pi}{\omega_0}\right)$. The inset is the absorption spectrum. For comparison, the absorption energy is scaled by a factor of $\frac{1}{\omega_0}$. Except the results in Figure 4, all other results are produced by using the ECP CRENBL with its matching orbital basis set for the valence electrons.

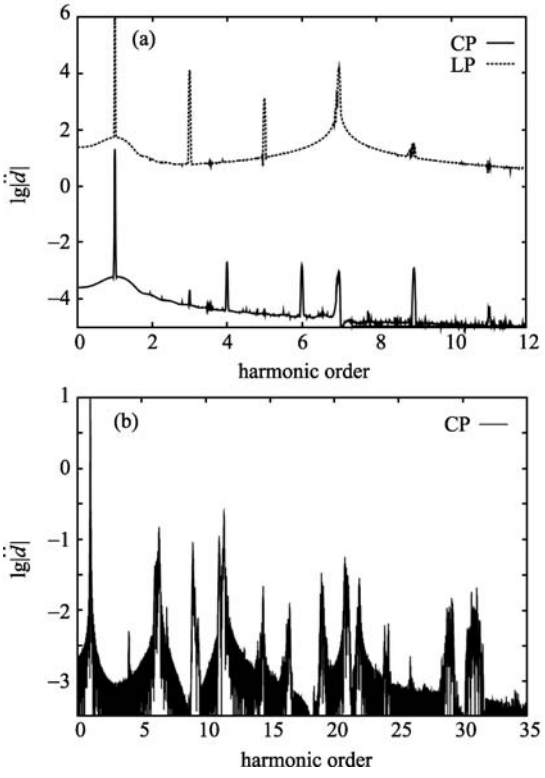

Figure 4 (a) Harmonics generated by C_{10} in LP and CP fields with $\omega_0 = 0.04$, $E_{\max} = 0.03$ and $t_p = 120\tau$. The overall harmonic spectrum of C_{10} in LP laser field is upwardly shifted by 4. (b) Harmonics generated by C_{10} in CP field with $\omega_0 = 0.04$, $E_{\max} = 0.05$ and $t_\mathrm{p} = 50\tau$. The Pople full-electron basis 6-31G** is applied to produce the results in this figure.

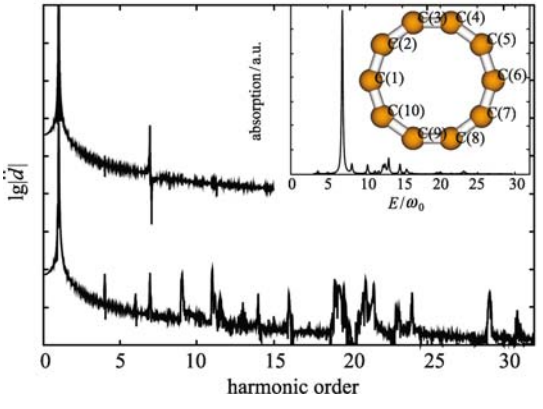

Figure 5 Harmonics generated by C_{10} in CP field with $\omega_0 = 0.04$ and $t_\mathrm{p} = 50\tau$. The field amplitude is changed from $E_{\max} = 0.01$ to 0.02. The inset is the absorption spectrum.

Unlike harmonic spectra in LP laser field, harmonics generated by C_{10} in CP laser field show quite different spectral characters (see Figures 4 and 5). They include both odd- and even-order harmonics. For instance, 4-th, 6-th, 9-th, 11-th, …, order harmonics are observed. The dynamical symmetry of the time periodic Hamiltonian combined with Floquet formalism has been applied to predict which order of harmonics are allowed in the cyclic molecules [105]. The approach assumed that the system driven by a periodically time-dependent field is in a pure field-dressed Floquet state. Therefore, the probability of getting the n-th harmonic in a Floquet state $\psi_W(\mathbf{r},t)$ of a system ($\psi_W(\mathbf{r},t) = \Phi(\mathbf{r},t)\mathrm{e}^{-\mathrm{i}Wt}$, where W is the quasi-energy, $\Phi(\mathbf{r},t+\tau) = \Phi(\mathbf{r},t)$, and $\tau = 2\hbar\pi/\omega$) can be written as

$$\sigma_W^n \propto n^4 \left| << \Phi(\mathbf{r},t) \left| \hat{\mu}\mathrm{e}^{-\mathrm{i}n\omega t} \right| \Phi(\mathbf{r},t) >> \right|^2, \qquad (51)$$

where the double braket notation, $<<...>>$, stands for the integration over spatial variables and time. When the Hamiltonian $\mathcal{H}(t) = H(t) - \mathrm{i}\dfrac{\partial}{\partial t}$ is invariant under dynamical symmetry of order N, Ref. [105] derived the HHG spectral selection rule: the n-th order harmonic emits only when n satisfies the condition $n = kN \pm 1$. Therefore, the higher the symmetry order N, the less the generated harmonics within a fixed frequency interval.

The point group of C_{10} belongs to D_{5h}. When it interacts with a CP laser pulse with sufficiently long duration, its molecular Hamiltonian has the symmetry group C_5. Therefore, one can derive the spectral SR: $n = 5k \pm 1$ for C_{10} with respect to the Floquet formalism. However, the system may not be in a pure field-dressed Floquet state for the subfemtosecond laser pulse. This may result in additional peaks other than those predicted from the spectral selection rule to be present [106,107]. For instance, the peak near the 7-th order appears in HHG spectra of C_{10} in both LP and CP field (see Figure 4) and the peak near 9-th order is observed in HHG spectra of C_9 in LP field.

To identify the origin of these additional peaks, we calculate the absorption spectra of C_9 and C_{10} in a relatively weak field ($E_{\max}$ = 0.001 a.u.). Comparing the HHG spectra with the absorption spectra, we observe that the additional peaks prefer to being generated near the positions with the excitation energies corresponding to the strongest absorption peaks. For example, the absorption peak with the excitation energy Δ = 7.56 eV and the transition dipole moment $|\mu|$ = 3.35 a.u. for C_{10} and that with Δ = 4.7 eV and $|\mu|$ = 6.4 a.u. for C_9. Lezius et al. called the excited state which is most strongly coupled to the ground state as the doorway state in Refs. [108,109]. Through it, electrons are excited to a quasicontinuum (QC) of excited-states. The QC is formed as the intense laser field shifts and mixes the energy levels of the excited-state manifold, thus allowing electrons to rapidly climb up and ionize. When the electron response to the laser field oscillation becomes nonadiabatic, Landau-Zener type nonadiabatic transitions become increasingly probable, allowing population to evolve towards higher-lying (bound) electronic states. At $\omega_0 E_{\max} L \sim \Delta^2$, this nonadiabatic transition that corresponds to charge transfer across the molecule is quickly saturated, leading to strong nonresonant absorption by all delocalized electrons involved in this coupling [108,109], where L is the characteristic length of system.

The electrons that transit to the doorway state via the nonresonant absorption may quickly go back to the ground state by emitting a radiation or rapidly climb up to QC and ionize. It is apparent that the peaks near 9-th order in HHG of C_9 and 7-th order in HHG of C_{10} are originated from the population of the doorway states. Because of fast saturation of the nonadiabatic transition, in this limit non-resonant energy absorption becomes only weakly sensitive to laser intensity. This explains the reason why the relative intensities of these additional peaks reduce (see the peak near 7-th order in Figure 4) as the field intensity increases. They may not be observed in the HHG spectra when one further increases the intensity of laser pulses. The ionization probabilities may be predicted by the nonadiabatic multi-electron (NME) theory [108,109]. The Landau-Zener-type nonadiabatic transition probability, defined as $P_{\mathrm{LZ}} \sim \exp(-\pi\Delta^2/(4\omega_0 E_{\max} L))$, respectively predicts an maximum ionization probability 2×10^{-5} and 1.7×10^{-3} for C_{10} at ω_0 = 0.04 a.u., $E_{\max}$ = 0.03 and 0.05 a.u. during one-half a laser cycle, where L is set to $\sqrt{2.0}\mu$ by considering the effect of LP pulses. It is apparent that NME predicts no significant ionization under the conditions of our simulations.

As $E_{\max}$ increases to 0.05 a.u., more higher-lying excited states can be populated and the ionization probability increases. Hence more electrons can be ionized. The ionized electrons recollide with the atomic nuclei and create additional emission channels even for molecular HHG in CP fields at this moderate laser intensity. The effect of basis set is checked. Figure 5 shows the harmonics generated by using ECP CRENBL with a matching orbital basis set for the valence electrons. Comparing HHG in Figure 4 and Figure 5, the effect of basis set on electron spectra is significant. Even with a weaker field $E_{\max}$ = 0.02 a.u., the maximum order harmonic generated by using ECP is same with that using the Pople basis set 6-31G** at $E_{\max}$ = 0.05 a.u.. Larger basis set including diffuse functions and continuum functions is expected to describe HHG of polyatomic molecules more exactly.

3.2 Electronic dynamics

In our RT-TDDFT scheme, TDDFT equation is solved by propagating the reduced density matrix in real-time domain. In the spectrum calculations, the initial density matrix $\rho(t \to -\infty)$ is obtained from a usual ground state calculation, i.e. $\rho(t = -\infty) = \rho_0$. Then, the external field interacts with the system, the system electron density $\rho(t)$ evolutes following the external field. One may plot the field-induced charge density to exhibit the electron coherence or population distribution in real space or in different molecular orbitals. Alternatively, one may propagate the reduced density matrix in realtime domain starting from other non-equilibrium states, for example, one of the excited states. Then one may study the pure dephasing time, or the population relaxing time, or time time-evolution of electron population in some blocks of molecules. In the follow we conduct one calculation for each case.

3.2.1 The laser-driven instantaneous electron population analysis

The detailed knowledge of the laser-driven electron dynamics can be obtained from the time evolution of the electronic density $\delta\rho(x,y,z,t) = \sum_\lambda \sum_\sigma \varphi_\lambda(x,y,z)\delta\rho'_{\lambda,\sigma}(t)\varphi_\sigma(x,y,z)$. The laser-induced density matrix $\delta\rho(t)$ is obtained by solving Eq. (9) in real-time domain. $\{\varphi_\lambda\}$ is the atomic orbital. Figure 6 depicts $\delta\rho$ on the xy plane, which is situated at middle of the (9, 0) BNNTs and includes B atoms only. $\delta\rho$ at different time within one optical cycle is demonstrated. Due to the large size of BNNT, we implemented the timedependent one-electron approach at HF level with the semi-empirical Hamiltonian INDO/S [101]. The data $\delta\rho$ offers the underlying information about the evolution of the electron wave function during

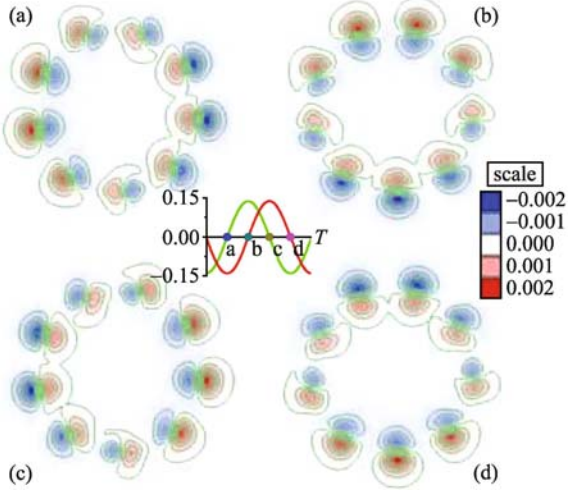

Figure 6 The 2-D charge density of (9, 0) $(BN)_{72}H_{18}$ at different time within one optical cycle in the CP field, ω_0 = 1.0 eV and t_p = 120τ.

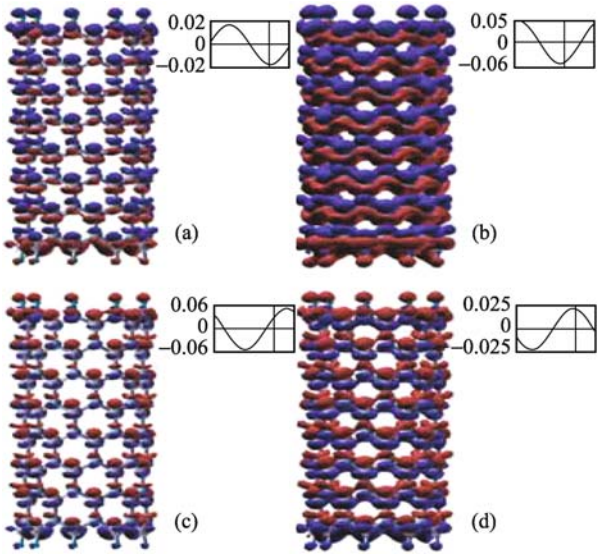

Figure 7 The 3-D charge density distribution of (9, 0) $(BN)_{72}H_{18}$ at the time interval of 100 fs in the LP field, ω_0 = 1.0 eV and t_p = 120τ .

harmonic generation. We find that the laser pulse drives the distribution of the induced charge density to alternate with the same frequency as the external field. One may expect to observe unidirectional valence-type electronic ring currents in NTs driven by a ultrashort CP laser pulse within the pulse duration, as Barth et al. have observed in the oriented molecule Mg-Porphyrin excited by a few of optical cycles CP UV π laser pulse [110,111]. In this work we only demonstrate that the π-electron rotation in achiral tubes is along the tube axis through a circularly polarized laser pulse. We may expect to observe the π-electron rotation in chiral tubes by nonhelical laser pulses.

The direction of the laser-induced polarization is determined by the polarization direction of the external field, which is further indicated by the induced charge density distribution of (9,0) BNNT when it interacts with a LP laser field polarized along the tube axis (see Figure 7). Because of the polarization of external field, the induced charge density is divided into negative and positive electron cloud, which distributes at the two sides of B and N atoms. The induced charge density increases as the field becomes strong. It forms many circles of positive and negative electron cloud, which appear alternatively along the tube axis of (9, 0) BNNTs in LP laser field. A charge current may be produced along the tube axis in (9, 0) BNNT.

3.2.2 Electron-injection dynamics in dye-sensitized TiO_2 clusters

Light-driven heterogeneous electron transfer (ET) is a fundamental process that plays an important role in interfacial

photoprocesses, particularly in photoelectrochemistry [112,113], photocatalysis [114], and molecular electronics for dye-sensitized solar cells (DSSCs) [115]. DSSC assembles organic dyes with inorganic semiconductor nanocrystals such as TiO_2, and realizes the optical absorption and charge-separation processes. Visible light excites the dyesensitizer molecules from the ground state to an excited state which is resonant with the TiO_2 conduction band. The excited electrons are then transferred to the semiconductor on an ultrafast timescale. This interfacial ET was shown to take place within 100 fs. It indicates that the ET is faster than vibration relaxation in this system. This ultrafast ET dynamics can not be well explained by traditional ET rate theory and requires a time-resolved femtosecond or subfemtosecond laser technique or real-time theoretical study.

In the following we demonstrate how to use RT-TDDFT to study the ultrafast ET process. We follow the evolution of the atomic electron population in time until the onset of nuclear motion-induced relaxation terminates the purely electronic coherent motion. Unlike the usual situation, the initial density matrix is obtained from a usual ground state calculation. In this study, the initial state is assumed as an excited state of dye molecules and the nanoparticle is in its ground state [116]. With this assumption, the ET process between the dye molecules and TiO_2 clusters is thought as a photo-induced ET process and the electron injection is regarded as electronic relaxation process at a very fast time scale, in which the nuclei are frozen in their equilibrium nuclear configurations. That is to say, the electrons re-optimize their locations after excitation of dyes whereas the nuclei have no time to move.

Then the number of electrons localized at dye molecules vs. the propagation time is evaluated by

$$N_{dye}(t) = \sum_{A\in dye}\sum_{\mu\in A}\sum_{\nu}^{N}\rho'_{u\nu}(t)S_{\nu\mu}. \quad (52)$$

In order to analyze the ET process, the number of electrons localized at dye molecules is fitted to a dual exponential function (see Figure 8), which includes the characteristic time of the motion of electrons, as

$$N_{dye}(t) = N_{dye}(t=0) + A_1\exp(-t/\tau_1) + A_2\exp(-t/\tau_2). \quad (53)$$

The τ_1 with a smaller value describes an ultrafast process of the early electronic redistribution of initial states with the time scale less than 1.0 fs, while τ_2 with a larger value corresponds to the lifetime of the initial states. Figure 8 displays the clear dependence of the ET time on the cluster sizes [116]. As the cluster sizes increase from $(TiO_2)_8$ to $(TiO_2)_{14}$, the τ_2 values decrease rapidly. Larger clusters $(TiO_2)_{14/16}$ show an ET time that is more consistent with the experimental measurements. Clusters $(TiO_2)_{14}$ and $(TiO_2)_{16}$ are small. It is thus expected that the τ value can reach a limited value when the cluster size is large enough.

The different initial states are used to propagate the reduced density matrix to show the influence of initial states on the ET event. As an example, pycooh's 1-st excited state (which nearly fully comes from the electron transitions from HOMO → LUMO). And 3-rd excited state (which comes mainly from HOMO – 1 → LUMO and HOMO – 3 → LUMO transitions) will be chosen to construct the different initial states. These two excited states are both optically active. It is observed that the electronic relaxing times starting from the different initial state are different. The initial state built from the 1-st excited state of pycooh favors a faster ET than the one built from the

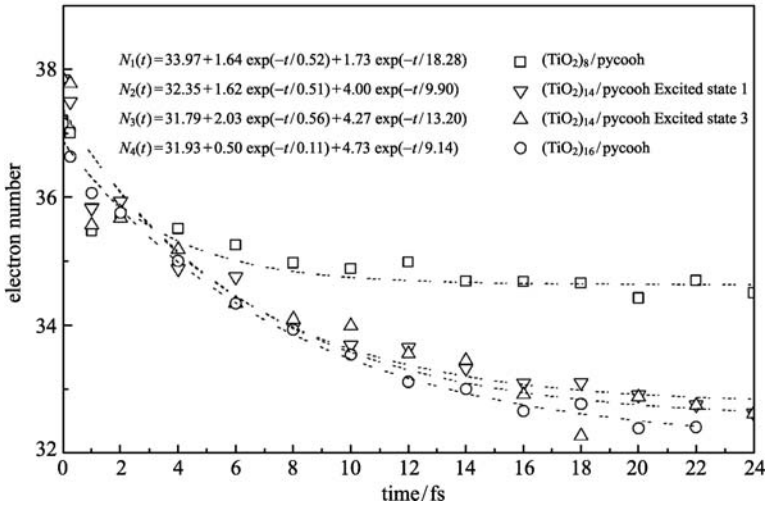

Figure 8 Electronic relaxation of the excited pycoohin the pycooh-$(TiO_2)_{(8/14/16)}$ systems. The number of *y*-axis represents the number of electrons localized in pycooh. The dashed lines denote the exponential fittings.

3-rd excited state of pycooh. From the orbital contributions of low-lying excited states for pycooh-$(TiO_2)_{14}$ system, we note that they come mainly from the orbital transitions from the occupied HOMO or HOMO − 1 of pycooh to the virtual orbitals of $(TiO_2)_{14}$. These states are the direct optical charge transfer states. Thus, the time scale of the direct optical ET is fastest in the ET process. The 3-rd excited state of pycooh involves the orbital contribution from HOMO − 3 → LUMO, which slows down the ET event between the excited pycooh and $(TiO_2)_{14}$. However, both initial states behave nearly the same time-dependent character since the contribution to the 3-rd excited state of pycooh from HOMO − 3 → LUMO transition is much smaller than that from HOMO − 1 → LUMO.

Our *ab initio* electron dynamics simulation gives evidence that the electron injection from the excited dyes to TiO_2 is an ultrafast process, and indicates that it is safe to ignore the nuclear movement for the present systems because its relaxation time is at about sub-picosecond. The ET process is significantly influenced by the cluster size when the cluster is small. However, the size effects on ET time reduce dramatically as the cluster size increases. A moderate middle size cluster $(TiO_2)_{14}$ has captured the essence of electronic relaxation of the excited dyes to TiO_2 cluster at an affordable computational cost.

3.2.3 Ehrenfest dynamics

In our HHG calculations, the nuclear geometry is freezed. It is interesting to see the influence of the nuclear motion on HHG. Kreibich et al. have studied HHG of HD beyond the Born-Oppenheimer (BO) approximation [117]. They found that when one does not take the nuclei motion into account, the emission HHG spectrum of HD is the same as that of H_2 because the real used parameter in BO-TDDFT is the charge of nuclei. Therefore in BO-TDDFT the effect of H and D is the same, and HD can still be thought to be inverse symmetrical. But when the nuclear motion is taken into account, the symmetry is broken and the even HHGs appear in the emission spectra (see Figure 9).

The time scale of electron motion usually lies within attosecond or subfemtosecond. For most heavy atoms the motion of nuclei is much slower than electron so that it hardly contribute to the HHG. But for the lightest atoms, such as H and D, the characteristic time of nuclear motion is much shorter, even extending to femtosecondscale so that molecular HHG can be affected by the motion of these light nuclei [35,118,119]. Figure 10 shows the time-dependent dipole $d(t)$ of H_2 exposed to strong laser field with different initial kinetic energy E_{kin}. When E_{kin} = 0, $d(t)$ obtained with Ehrenfest

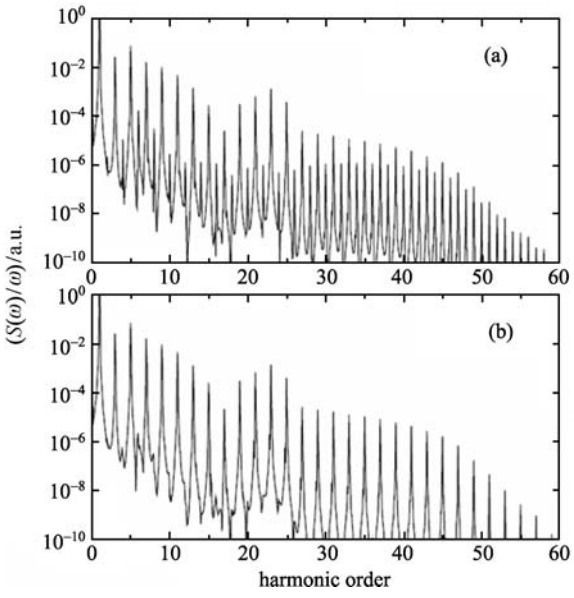

Figure 9 (a) Harmonic spectrum generated from the model HD molecule driven by a laser with peak intensity of 10^{14} W·cm^{-2} and wavelength of 770 nm. The plotted quantity is proportional to the number of emitted photons. (b) Same as panel (a) for the model H_2 molecule [117].

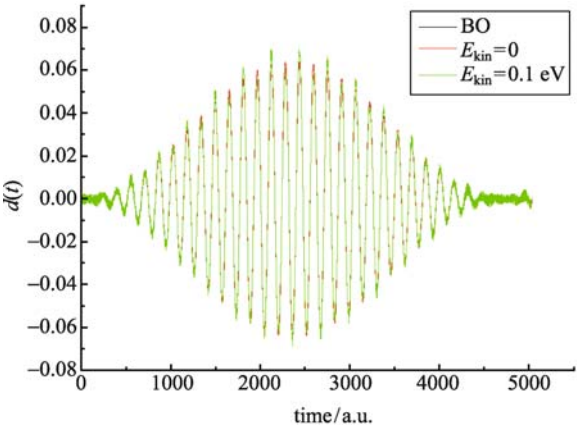

Figure 10 The calculated time-dependent dipole $d(t)$ with different initial kinetic energy. BO refers to BO-TDDFT and the other two refer to Ehrenfest dynamics.

dynamics is the same as with BO-TDDFT. When E_{kin} = 0.1 eV, the time-dependent dipole $d(t)$ deviates from the result of BO-TDDFT although they are exposed to the same external laser field. At this case, $d(t)$ oscillates in the initial stage because of the motion of H atom, and after the field is turned off, $d(t)$ continue oscillating,i.e., $d(t)$ doesn't adjusts instantaneously to the time-varying electric field $E(t)$ of the laser. The nonadiabatic effect starts to show on $d(t)$.

In the dynamical processes, such as laser-induced chemistry, dynamics at metal or semiconductor surfaces, and

electron transfer, the quantal electrons do not evolve adiabatically, which leads to non-BO trajectories for nuclear motion. People combine RT-TDDFT scheme with Ehrenfest dynamics or surface hopping dynamics to study nonadiabatic dynamics.

For example, Li et al. used *ab initio* Ehrenfest dynamics to study the rotation of $H_2C=NH_2^+$ [40–44]. The natural charges of the NH_2 group are calculated as a function of the torsional angle with BO Dynamics and Ehrenfest Dynamics in Figure 11. The breaking and reformation of the relatively rigid π bond always accompany the rotation of a covalent double bond. In the avoided crossing region, the strong electron-nuclear coupling can result in an electronic nonadiabatic transition so that molecules are excited. Such a phenomenon cannot be simulated by the adiabatic BO molecular dynamics while Ehrenfest Dynamics can finish it. The nonadiabatic transition leads to the oscillation of charge. When nuclear kinetic energy becomes higher, the nonadiabatic behavior becomes more pronounced.

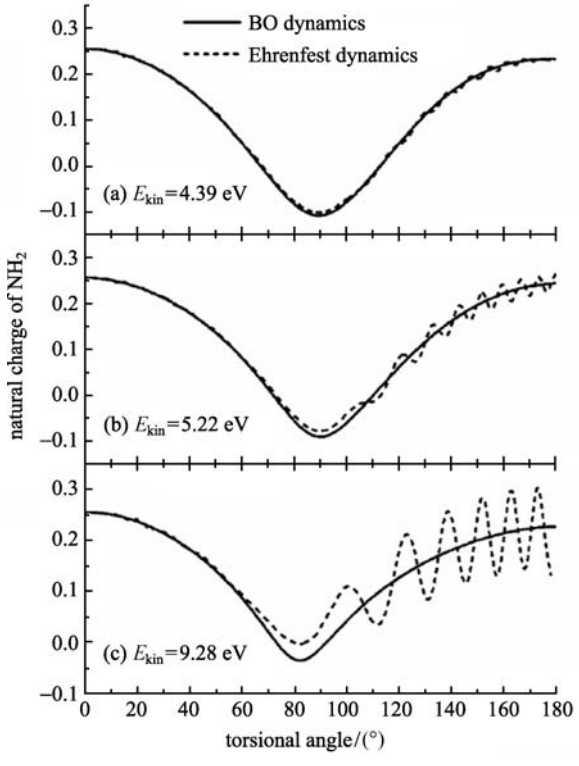

Figure 11 Dynamics of $H_2C=NH_2^+$ internal rotation about the double bond with different initial torsional kinetic energies.

3.3 Problems in TDDFT

In the above applications, TDDFT is used to study the electron excitation, ionization and interface charge transfer etc. But TDDFT with the conventional XC functionals (even the popular hybrid XC functionals such as B3LYP) has been found to provide a poor description to the polarizabilities of large extended $\pi-$conjugated systems, the long-range intermolecular CT excitations and the high Rydberg states due to the known problems on the nonlocality and asymptotic behavior of available density functionals [120–123]. For example, the conventional TDDFT usually underestimates excitation energy below the TDDFT ionization threshold and underestimates excitations with little or no charge density relaxation (charge transfer excitations are underestimated by 1 or 2 eV). These problems originate from the inaccurate DFT energy functional E_{xc}, the wrong asymptotic behavior of υ_{xc}, or the adiabatic approximation, etc.

For example the approximate XC functionals usually gives rise to the self-interaction (SI) energy. A promising procedure for removing the self-interaction energy in steady-state DFT treatments is based on the extension of the Krieger-Li-Iafrate (KLI) semianalytic treatment [124] of the optimized effective potential (OEP) formalism [125,126] along with the use of either the Hartree exchange [124,127] or an explicit self-interaction-correction (SIC) form [128]. The OEP so constructed has the proper long-range asymptotic $-1/r$ behavior and is capable of providing high accuracy for both excited and autoionizing resonance states. Tong and Chu combined the TD-KLI and SIC scheme to derive a TDKLI-SIC scheme for a nonperturbative study of HHG of He atoms in intense laser fields [129]. They calculated the HHG of He atom by means of two different schemes. Figure 12 showed the comparison of the HHG power spectra of He atoms obtained from the TDKLI-SIC-LDA (filled circles) and ALDA (open circles). It is obvious that the HHG cutoff order of ALDA is smaller than that of TDKLI-SIC-LDA. The severe underestimation of the ionization energy of atom leads to smaller cutoff order.

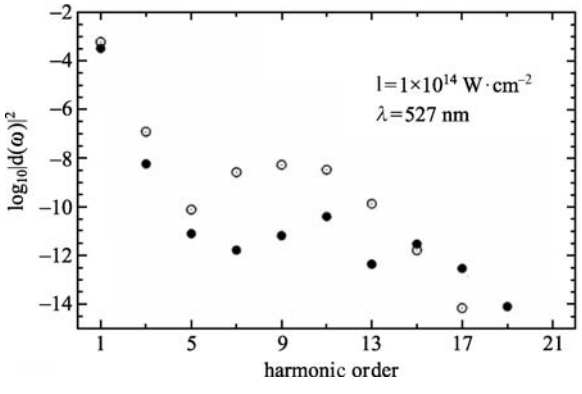

Figure 12 Comparison of the HHG spectra of He atoms calculated by ALSDA (open circles) and TD-CKLI-SIC-LSDA (filled circles) methods. The laser intensity used is 1×10^{14} W·cm^{-2} and the wavelength used is 527 nm [129].

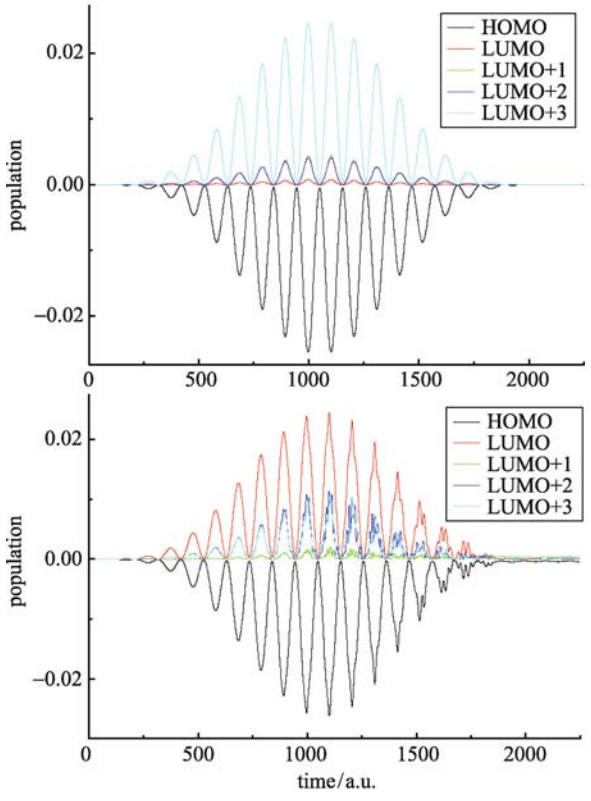

Figure 13 The time-dependent population of C_2H_4 calculation with XC functionals LRC-PBEOP (μ = 0.33/a_0)(top panel) and PBEOP (bottom panel).

Most recently motivated by the observation that nonlocal HF exchange potentials properly describes the distance dependence of long-range CT excited states and the polarizabilities of extended π-conjugated systems, people implement the range-dependent nonlocal HF exchange, which splits the two-electron operator r_{12}^{-1} into a short- and a long-range part

$$\frac{1}{r} = \frac{1-erf(\mu r)}{r} + \frac{erf(\mu r)}{r}, \tag{54}$$

leading to the long-range-corrected DFT scheme [130–145]. Here *erf* denotes the error function, μ is considered to be an adjustable parameter, which is introduced to determine the length scale over which the HF exchange is turned on.

The preformation of LRC-DFT scheme has been systematically accessed on the calculation of ground-state properties and excitation energies. However, the performance of LRC-DFT on the strong field electronic dynamic, in which the motion of electron is far away from nuclei and the long-range interaction becomes more obvious, is rarely reported. Here we check the effect of the long range correction to XC functionals on the intense field phenomena. We calculate the time-dependent population of C_2H_4 exposed to the linearly-polarized external pulse with ω = 0.03 a.u., τ_p = 30τ, E_{max} = 0.05 a.u.. Both the conventional functional PBEOP [146] and LRC-PBEOP(μ = 0.3/a_0, a_0: the bohr radius) functional are used. The basis set 6-31G is employed. We find that two functionals produce two significantly different results. TD-LRC-PBEOP results show, when the external field interacts with C_2H_4, more electrons are populated to higher unoccupied orbitals whileas TD-PBEOP results show electrons are mainly populated on LUMO, LUMO + 1 and LUMO + 2. In the same external field, the function of population oscillates with the time after several optical cycles for PBEOP functional while when LRC-PBEOP functional is used, the function of population changes smoothly with the time. It seems that the approximate functional PBEOP produces v_{xc} which underbind the electrons because the potentials go too rapidly to zero at large distance. In this case, the nonadiabatic multielectron effect is pronounced, which gives rise to the higher-lying (bound) electronic states populated during the laser duration and results in small oscillations in $d(t)$. Furthermore, these higher-lying excited states remain populated after the pulse passes over. Therefore, $d(t)$ keeps oscillations and do not return to zero when the field is turned off.

In the intense-filed electronic dynamics, the motion of electrons is usually far away from nuclei. Therefore, the long range correction to the conventional XC functionals is crucial and LRC-DFT can provide a more reliable tool to study the intense field phenomena and electron excitation of large extended π−conjugated systems.

4 Conclusions

In summary, RT-TDDFT becomes a promising tool to study the time-dependent phenomena and the dynamical properties of large-size systems as we demonstrate in the above sections. It overcomes the limitation of LR-TDDFT and can be used to study the intense field phenomena and non-BO dynamics. Comparing to DFT for the stationary ground state problem, TDDFT for the excited-state problem is far less perfect because of the existing problem on DFT XC functionals and the intrinsic failure of ALDA. Large improvements are essential. Therefore one should use TDDFT with care especially when TDDFT is used to study the problems like the above-threshold ionization, multiphoton ionization, the long-range electron excitation, and the materials like polyenes and free radicals, etc.

Acknowledgements Financial supports from the National Science Foundation of China (Grant Nos. 20673104 and 20833003), the National Basic Research Program of China (Grant Nos. 2004CB719901 and 2006CB922004) and Chinese Academy of Science are acknowledged.

Wanzhen LIANG got her degree of B.S. in 1987 from Department of Physics at University of Southwest Normal University and her Ph.D. degree in 2001 from Department of Chemistry at University of Hong Kong. She was a postdoctoral Fellow in Department of Chemistry and Department of Chemical Engineering at University of California at Berkeley. She worked as a professor in Department of Chemical Physics and Hefei National Laboratory for Physical Science at Mircoscale at University of Science and Technology of China since September 2003. Her group's current research activities are focused on the developments and applications of electronic structure theory and fast numerical methods to study the electronic spectroscopy and dynamics of complex systems.

References

1. Runge, E.; Gross, E. K. U., *Phys. Rev. Lett*. **1984**, *52*, 997–1000
2. Marques M. A. L.; Gross, E. K. U., *Annu. Rev. Phys. Chem*. **2004**, *55*, 427–455
3. Ring, P.; Schuck, P., *The Nuclear Many-body Problem*, Springer: New York, 1980
4. Casida, M. E., *Recent Advances in Density Functional Methods, Part I*, World Scientific: Singapore, 1995
5. Casida, M. E., *Recent Developments and Applications in Density Functional Theory*, Elsevier: Amsterdam, 1996
6. Hirata, S.; Head-Gordon, M., *Chem. Phys. Lett*. **1999**, *314*, 291–299
7. Zangwill, A.; Soven, P., *Phys. Rev. A* **1980**, *21*, 1561–1572
8. Nuroh, K.; Sott, M. J.; Zaremba, E., *Phys. Rev. Lett*. **1982**, *49*, 862–866
9. Mahan, G. D., *J. Chem. Phys*. **1982**, *76*, 493–497
10. Baroni, S.; Giannozzi, P.; Testa, A., *Phys. Rev. Lett*. **1987**, *58*, 1861–1864
11. Levine Z. H.; Allan, D. C., *Phys. Rev. Lett*. **1989**, *63*, 1719–1722
12. Yabana, K.; Bertsch, G. F., *Phys. Rev. B* **1996**, *54*, 4484–4487
13. Rubio, A.; Alonso, J. A.; Blase, X.; Balbas, L. C.; Louie, S. *G., Phys. Rev. Lett*. **1996**, *77*, 247–250
14. van Gisbergen, S. J. A.; Snijders, J. G.; Baerends, E. J., *Phys. Rev. Lett*. **1997**, *78*, 3097–3100
15. Shukla, M. K.; Leszczynski, J., *J. Phys. Chem. A* **2004**, *108*, 10367–10375
16. Rogers, J. E.; Nguyen, K. A.; Hufnagle D. C.; McLean, D. G.; Su, W. J.; Gossett, M.; Burke, A. R.; Vinogradov, S. A.; et al., *J. Phys. Chem. A*, **2003**, *107*, 11331–11339
17. Furche, F.; Ahlrichs, R., *J. Chem. Phys*. **2002**, *117*, 7433–7447
18. Scalmani, G.; Frisch, M. J.; Mennucci, B.; Tomasi, J.; Cammi, R.; Barone, V., *J. Chem. Phys*. **2006**, *124*, 094107
19. Krausz, F.; Ivanov, M., *Rev. Mod. Phys*. **2009**, *81*, 163–234
20. Agostini, P.; Fabre, F.; Mainfray, G.; Petite, G.; Rahman, N. K., *Phys. Rev. Lett*. **1979**, *42*, 1127–1130
21. Ferray, M.; L'Huillier, A.; Li, X. F.; Lempre, L. A.; Mainfray, G.; Manus, C., *J. Phys. B* **1988**, *21*, L31–L35
22. Jahnke, T.; Czasch, A.; Schöffler, M. S.; Schössler, S.; Knapp, A.; Kösz, M.; Titze, J.; Wimmer, C.; et al., *Phys. Rev. Lett*. **2004**, *93*, 163401
23. Bucksbaum, P. H., *Science* **2007**, *317*, 766–769
24. Goulielmkis, E.; Yakovlev, V. S.; Cavalieri, A. L.; Uiberacker, M.; Pervak, V.; Apolonski, A.; Kienberger, R.; Kleineberg, U.; et al., *Science* **2007**, *317*, 769–775
25. Kapteyn, H.; Cohen, O.; Christov, I.; Murnane, M., *Science* **2007**, *317*, 775–778
26. Calvayrac, F.; Reinhard, P. G.; Suraud, E.; Ullrich, C. A., *Phys. Reports* **2000**, *337*, 493–578
27. Kling, M. F.; Vrakking, M. J. J., *Ann. Rev. Phys. Chem*. **2008**, *59*, 463–492
28. Winterfeldt, C.; Spielmann, C.; Gerber, G., *Rev. Mod. Phys*. **2008**, *80*, 117–140
29. Farkas, G.; Toth, C., *Phys. Lett. A* **1992**, *168*, 447–450
30. Antoine, P.; L'Huillier, A.; Lewenstein, M., *Phys. Rev. Lett*. **1996**, *77*, 1234–1237
31. Antoine, P.; Milosevic, D. B.; L'Huillier, A.; Gaarde, M. B.; Salieres, P.; Lewenstein, M., *Phys. Rev. A*, **1997**, *56*, 4960–4969
32. Harris, S. E.; Sokolov, A. V., *Phys. Rev. Lett*. **1998**, *81*, 2894–2897
33. Corkum, P. B., *Phys. Rev. Lett*. **1993**, *71*, 1994–1997
34. Hay, N.; Nalda, R. de; Halfmann, T.; Mendham, K. J.; Mason, M. B.; Castillejo, M.; Marangos, J. P., *Eur. Phys. J. D* **2001**, *14*, 231–240
35. Baker, S.; Robinson, J. S.; Haworth, C. A.; Teng, H.; Smith, R. A.; Chirila, C. C.; Lein, M.; Tisch, J. W. G.; et al., *Science* **2006**, *312*, 424–427
36. Wagner, N. L.; Wuest, A.; Christov, I. P.; Popmintchev, T.; Zhou, X; Murnane, M. M.; Kapteyn, H. C., *Proc. Nat. Aca. Sci*. **2006**, *103*, 13279–13285
37. Zhang, G. P., *Phys. Rev. Lett*. **2005**, *95*, 047401
38. Averbukh, V.; Alon, O. E.; Moiseyev, N., *Phys. Rev. A* **2001**, *64*, 033411
39. Baer, R.; Neuhauser, D.; Zdanska, P. R.; Moiseyev, N., *Phys. Rev. A*, **2003**, *68*, 043406
40. Li, X. S.; Tully, J. C.; Schlegel, H. B.; Frisch, M. J.. *J. Chem. Phys*. **2005**, *123*, 084106
41. Li, X. S.; Smith, S. M.; Markevitch, A. N.; Romanov, D. A.; Levis, R. J.; Schlegel, H. B., *Phys. Chem. Chem. Phys*. **2005**, *7*, 233–239
42. Isborn, C. M.; Li, X. S.; Tully, J. C., *J. Chem. Phys*. **2007**, *126*, 134307
43. Schlegel, H. B.; Smith, S. M. ; Li, X. S., *J. Chem. Phys*. **2007**, *126*, 244110
44. Smith, S. M.; Li, X. S.; Markevitch, A.; Romanov, D.; Levis, R. J.; Schlegel, H. B., *J. Phys. Chem. A* **2007**, *111*, 6920–6932
45. Castro, A.; Marques, M. A. L.; Alonso, J. A.; Bertsch, G. F.; Rubio, A., *Eur. Phys. J. D* **2004**, *28*, 211–218
46. Isborn, C. M.; Li, X.; Tully, J. C., *J. Chem. Phys*. **2007**, *126*,

134307
47. Tully, J. C., *Dynamics of Molecular Collisions Vol. 2*, New York: Plenum, 1976, p. 217
48. Tully, J. C., *J. Chem. Phys*. **1990**, *93*, 1061–1071
49. Parandekar, P. V.; Tully, J. C., *J. Chem. Phys*. **2005**, *122*, 094102
50. Craig, C. F.; Duncan, W. R.; Prezhdo, O. V., *Phys. Rev. Lett.*, **2005**, *95*, 163001
51. Yam, C. Y.; Yokojima, S.; Chen, G. H., *Phys. Rev. B* **2003**, *68*, 153105
52. Yam, C. Y.; Yokojima, S.; Chen, G. H., *J. Chem. Phys*. **2003**, *119*, 8794–8803
53. Wang, F.; Yam, C. Y.; Chen, G. H.; Fan, K., *J. Chem. Phys*. **2007**, *126*, 134104
54. Castro, A.; Marques, M. A. L.; Rubio, A., *J. Chem. Phys*. **2004**, *121*, 3425–3433
55. Yabana, K.; Nakatsukasa, T.; Iwata, J. I.; Bertsch, G. F., *Phys. Status Solidi B* **2006**, *243*, 1121–1138
56. Cheng, C. L.; Evans, J. S.; Voorhis, T. V., *Phys. Rev. B* **2006**, *74*, 155112
57. Pi, M.; Ancilotto, F.; Lipparini, E.; Mayol, R., *Physica E* **2004**, *24*, 297–307
58. Marques, M. A. L.; Castro, A.; Bertsch, G. F.; Rubio, A., *Comput. Phys. Commun*. **2003**, *151*, 60–78
59. Baer, R., *Phys. Rev. A* **2000**, *62*, 063810
60. Baer, R.; Gould, R., *J. Chem. Phys*. **2001**, *114*, 3385–3392
61. Baer, R.; Kurzwell, R.; Cederbaum, L. S., *Israel J. Chem*. **2005**, *45*, 161–170
62. Tsolakidis, A.; Sánchez-Portal, D.; Martin, R. M., *Phys. Rev. B* **2002**, *66*, 235416
63. Livshits, E.; Baer, R., *J. Phys. Chem*. **2006**, *110*, 8443–8450
64. Gordon, A.; Kartner, F. X,; Rohringer, N.; Santra, R., *Phys. Rev. Lett*. **2006**, *96*, 223902
65. Onida, G.; Reining, L.; Rubio, A., *Rev. Mod. Phys*. **2002**, *74*, 601–659
66. Burke, K.; Werschnik, J.; Gross, E. K. U., *J. Chem. Phys*. **2005**, *123*, 062206
67. Lein, M.; Kreibich, T.; Gross, E. K. U.; Engel, V., *Phys. Rev. A* **2002**, *65*, 033403
68. Pronin, K. A.; Bandrauk, A. D., *Phys. Rev. Lett*. **2006**, *97*, 020602
69. Suzuki, M., *J. Phys. Soc. Jpn*. **1993**, *61*, L3015–L3019
70. Sugino, O.; Miyamoto, Y., *Phys. Rev. B* **1999**, *59*, 2579–2586
71. Chu, S. I., *J. Chem. Phys*. **2005**, *123*, 62207
72. Chu, S. I.; Telnov, D. A., *Phys. Rep*. **2004**, *390*, 1–131
73. Chu, X.; Chu, S. I., *Phys. Rev. A* **2004**, *70*, 061402
74. Guan, X. X.; Tong, X. M.; Chu, S. I., *Phys. Rev. A* **2006**, *73*, 23403
75. Telnov, D. A.; Chu, S. I., *Phys. Rev. A* **2005**, *71*, 13408
76. Usachenko, V. I.; Chu, S. I., *Phys. Rev. A* **2005**, *71*, 63410
77. Manschwetus, B.; Nubbemeyer, T.; Gorling, K.; Steinmeyer, G.; Eichmann, U.; Rottke, H.; Sandner, W., *Phys. Rev. Lett*. **2009**, *102*, 113002
78. Bandrauk, A. D.; Ullrich, C., *Time-Dependent Density Functional Theory-New Developments*, Springer: New York, 2007
79. Ullrich, C. A.; Tokatly, I. V., *Phys. Rev. B* **2006**, *73*, 235102
80. Kurzweil, Y.; Baer, R., *J. Chem. Phys*. **2004**, 121, 8731–8741
81. Liang, W. Z.; Yokojima, S.; Chen, G. H., *J. Chem. Phys*. **1999**, *110*, 1844–1855
82. Liang, W. Z.; Saravanan, C.; Shao, Y.; Baer, R.; Bell, A. T.; Head-Gordon, M., *J. Chem. Phys*. **2003**, *119*, 4117–4125
83. Kosloff, R., *J. Phys. Chem*. **1988**, *92*, 2087–2100
84. Hu, W.; Schatz, G. C., *J. Chem. Phys*. **2006**, *125*, 132301
85. Sun, J.; Song, J.; Zhao, Y.; Liang, W. Z., *J. Chem. Phys*. **2007**, *127*, 234107
86. Lauvergnat, D.; Blasco, S.; Chapuisat, X.; Nauts, A., *J. Chem. Phys*. **2007**, *126*, 204103
87. Pollard, W. T.; Friesner, R. A., *J. Chem. Phys*. **1994**, *100*, 5054–5065
88. Press, W. H.; Teukolsky, S. A.; Vetterling, W. T.; Flannery, B. P., *Numerical Recipes in Fortran 90, 2nd Ed.*; Cambridge University Press: London, 1996
89. Blanes, S.; Casas, F.; Ros, J., *BIT* **2002**, *42*, 262–284
90. Magnus, W., *Pure Appl. Math*. **1954**, *7*, 649–673
91. Diele, F.; Lopez, L.; Peluso, R., *Adv. Comput. Math*. **1998**, *8*, 317–334
92. Watanabe, N.; Tsukada, M., *Phys. Rev. E* **2002**, *65*, 036705
93. Liang, W. Z.; Baer, R.; Saravanan, C.; Shao, Y. H.; Bell, A. T.; Head-Gordon, M., *J. Comp. Phys*. **2004**, *194*, 575–587
94. Iyengar, S. S.; Schlegel, H. B.; Millam, J. M.; Voth, G. A.; Scuseria, G. E.; Frisch, M. J., *J. Chem. Phys*. **2001**, *115*, 10291–1030
95. Liang, W. Z.; Yokojima, S.; Chen, G. H., *J. Chem. Phys*. **2000**, *113*, 1403–1408
96. Mitas, L.; Therrien, J.; Twesten, R.; Belomoin, G.; Nayfeh, M. H., *Appl. Phys. Lett*. **2001**, *78*, 1918–1920
97. Wadt, W. R.; Hay, P. J., *J. Chem. Phys*. **1985**, *82*, 284–298
98. Shao, Y.; Molnar, L. F.; Jung, Y.; Kussmann, J.; Ochsenfeld, C.; Brown, S. T.; Gilbert, A. T. B.; Slipchenko, L. V.; et al., *Phys. Chem. Chem. Phys*. **2006**, *8*, 3172–3191
99. Jackson, J. D. *Classical Electrodynamics 2nd Ed.*; Wiley-VCH: New York, 1975
100. Sun, J.; Guo, Z.; Liang, W. Z., *Phys. Rev. B* **2007**, *75*, 195438
101. Sun, J.; Liang, W. Z., Liu, Y., *J. Theo. Comp. Chem*. **2008**, *7*, 579–593
102. Sun, J.; Liu, J.; Liang, W. Z.; Zhao, Y., *J. Phys. Chem*. **2008**, *112*, 10442–10447
103. Stephens, P. J.; Devlin, F. J.; Chabalowski, C. F.; Frisch, M. J., *J. Phys. Chem*. **1994**, *98*, 11623–11627
104. Pacios, L. F.; Christiansen, P. A., *J. Chem. Phys*. **1985**, *82*, 2664–2671
105. Alon, O. E.; Averbukh, V.; Moiseyev, N., *Phys. Rev. Lett*. **1998**, *80*, 3743–3746
106. Moiseyev, N.; Lein, M., *J. Phys. Chem. A* **2003**, *107*, 7181–7188
107. Bavli, R.; Metiu, H., *Phys. Rev. A* **1993**, *47*, 3299–3310

108. Lezuis, M.; Blanchet, V.; Ivanov, M. Y.; Stolow, A., *J. Chem. Phys*. **2002**, *117*, 1575–1588
109. Lezuis, M.; Blanchet, V.; Rayner, D. M.; Villeneuve, D. M.; Stolow, A.; Ivanov, M. Y., *Phys. Rev. Lett*. **2001**, *86*, 51–54
110. Barth, I.; Manz, J.; Shigeta, Y.; Yagi, K., *J. Am. Chem. Soc*. **2006**, *128*, 7043–7049
111. Barth, I.; Manz, J., *Angew. Chem. Int. Ed*. **2006**, *45*, 2962–2965
112. Burfeindt, B.; Hannappel, T.; Storck, W.; Willig, F., *J. Phys. Chem*. **1996**, *100*, 16463–16465
113. Onda, K.; Li, B.; Zhao, J.; Jordan, K. D.; Yang, J. L.; Petek, H., *Science* **2005**, *308*, 1154–1158
114. ORegan, B.; Grätzel, M., *Nature* **1991**, *353*, 737–740
115. Grätzel, M., *Nature*, **2001**, *414*, 338–344
116. Guo, Z. Y.; Liang, W. Z.; Zhao, Y.; Chen, G. H., *J. Phys. Chem. C* **2008**, *112*, 16655–16662
117. Kreibich, T.; Lein, M.; Engel, V.; Gross, E. K. U., *Phys. Rev. Lett*. **2001**, *87*, 103901
118. Marangos, J. P.; Baker, S.; Kajumba, N.; Robinson, J. S.; Tisch, J. W. G.; Torres, R., *Phys. Chem. Chem. Phys*. **2008**, *10*, 35–48
119. Lein, M., *Phys. Rev. Lett*. **2005**, *94*, 053004
120. Cai, Z. L.; Sendt, K.; Reimers, J. R., *J. Chem. Phys*. **2002**, *117*, 5543–5549
121. Dreuw, A.; Head-Gordon, M., *Chem. Rev*. **2005**, *105*, 4009–4037
122. Dreuw, A.; Head-Gordon, M., *J. Am. Chem. Soc*. **2004**, *126*, 4007–4016
123. Dreuw, A.; Weisman, J. L.; Head-Gordon, M., *J. Chem. Phys*. **2003**, *119*, 2943–2946
124. Tong X. M.; Chu, S. I., *Phys. Rev. A*. **2001**, *64*, 013417
125. Krieger, J. B.; Li, Y.; Iafrate, G. J., *Phys. Lett. A* **1990**, *146*, 256–260
126. Sharp, R. T.; Horton, G. H., *Phys. Rev*. **1953**, *90*, 317–317
127. Talman, J. D.; Shadwick, W. F., *Phys. Rev. A* **1976**, *14*, 36–40
128. Grabo, T.; Gross, E. K. U., *Chem. Phys. Lett*. **1995**, *240*, 141–150
129. Tong, X. M.; Chu, S. I., *Phys. Rev. A* **1997**, *55*, 3406–3416
130. Leininger, T.; Stoll, H.; Werner, H. J.; Savin, A., *Chem. Phys. Lett*. **1997**, *275*, 151–160
131. Toulouse, J.; Colonna, F.; Savin, A., *J. Chem. Phys*. **2005**, *122*, 014110
132. Ángyán, J. G.; Gerber, I. C.; Savin, A.; Toulouse, J., *Phys. Rev. A* **2005**, *72*, 012510
133. Goll, E.; Werner, H. J.; Stoll, H., *Phys. Chem. Chem. Phys*. **2005**, *7*, 3917–3923
134. Goll, E.; Werner, H. J.; Stoll, H.; Leininger, T.; Gori-Giorgi, P.; Savin, A., *Chem. Phys*. **2006**, *329*, 276–282
135. Iikura, H.; Tsuneda, T.; Yanai, T.; Hirao, K., *J. Chem. Phys*. **2001**, *115*, 3540–3544
136. Tawada, Y.; Tsuneda, T.; Yanagisawa, S.; Yanai, T.; Hirao, K., *J. Chem. Phys*. **2004**, *120*, 8425–8433
137. Gerber, I. C.; Ángyán, J. G., *Chem. Phys. Lett*. **2005**, *415*, 100–105
138. Gerber, I. C.; Ángyán, J. G.; Marsman, M.; Kresse, G., *J. Chem. Phys*. **2007**, *127*, 054101
139. Vydrov, O. A.; Heyd, J.; Krukau, A. V.; Scuseria, G. E., *J. Chem. Phys*. **2006**, *125*, 074106
140. Vydrov, O. A.; Scuseria, G. E., *J. Chem. Phys*. **2006**, *125*, 234109
141. Song, J. W.; Hirosawa, T.; Tsuneda, T.; Hirao, K., *J. Chem. Phys*. **2007**, *126*, 154105
142. Cohen, A. J.; Mori-Sánchez, P.; Yang, W., *J. Chem. Phys*. **2007**, *126*, 191109
143. Chai, J. D.; Head-Gordon, M., *J. Chem. Phys*. **2008**, *128*, 084106
144. Chai, J. D.; Head-Gordon, M., *Chem. Phys. Lett*. **2008**, *467*, 176–178
145. Chai, J. D., Head-Gordon, M., *Phys. Chem. Chem. Phys*. **2008**, *10*, 6615–6620
146. Tsuneda, T.; Suzumura, T.; Hirao, K., *J. Chem. Phys*. **1999**, *110*, 10664–10678